Research Article

Yang Liu and Yi Zheng*

Reverse-switching radiative cooling for synchronizing indoor air conditioning

https://doi.org/10.1515/nanoph-2023-0699
Received October 15, 2023; accepted January 23, 2024;
published online February 1, 2024

Abstract: Switchable radiative cooling based on the phase-change material vanadium dioxide (VO_2) automatically modulates thermal emission in response to varying ambient temperature. However, it is still challenging to achieve constant indoor temperature control solely using a VO_2-based radiative cooling system, especially at low ambient temperatures. Here, we propose a reverse-switching VO_2-based radiative cooling system, assisting indoor air conditioning to obtain precise indoor temperature control. Unlike previous VO_2-based radiative cooling systems, the reverse VO_2-based radiative cooler turns on radiative cooling at low ambient temperatures and turns off radiative cooling at high ambient temperatures, thereby synchronizing its cooling modes with the heating and cooling cycles of the indoor air conditioning during the actual process of precise temperature control. Calculations demonstrate that our proposed VO_2-based radiative cooling system significantly reduces the energy consumption by nearly 30 % for heating and cooling by indoor air conditioning while maintaining a constant indoor temperature, even surpassing the performance of an ideal radiative cooler. This work advances the intelligent thermal regulation of radiative cooling in conjunction with the traditional air conditioning technology.

Keywords: reverse radiative cooling; phase-change material; indoor air conditioning; synchronized heating and cooling; precise temperature control

1 Introduction

In recent years, energy consumption has shown a steady rise alongside rapid economic development [1]. Heating and cooling systems in buildings are pivotal in providing a comfortable indoor environment, contributing to approximately 40 % of the total energy consumption in these structures [2], [3]. Consequently, it is crucial to prioritize the development of energy-efficient thermal technologies for energy conservation applications [4]. Take cooling for example, passive radiative cooling without energy consumption has emerged as an appealing approach for improving building heat dissipation by radiating heat from cooling materials installed on exterior walls into the ultracold outer space through the atmospheric transparent window (8–13 μm) and reflecting sunlight (0.3–2.5 μm) at the same time [5]–[15]. To obtain high-performance radiative cooling, a variety of cooing materials and structures with high solar reflectance (R_{solar}, $\lambda \sim 0.3$–$2.5\,\mu\mathrm{m}$) and high infrared emissivity ($\varepsilon_{\mathrm{ir}}$, $\lambda \sim 8$–$13\,\mu\mathrm{m}$) within the atmospheric transparent window have been proposed, including bio-inspired structures [16]–[20], film-based structures [21], [22], pigmented paint films [23]–[25], particle-based structures [24]–[28], as well as multilayer-film [5], [29]–[32] and patterned-surface photonic structures [33]–[37].

Although these radiative cooling structures exhibit highly efficient all-day cooling performance due to the static spectral characteristics, their fixed radiative cooling can cause overcooling effects on cold days, thereby resulting in additional heating costs. In response to the changing ambient temperature, some research has focused on switchable radiative cooling systems utilizing the phase change material vanadium dioxide (VO_2) to avoid the overcooling consequences [38]–[42]. In these studies, VO_2-based radiative coolers can automatically modulate their infrared emissivity based on the phase change of VO_2, where the radiative coolers enhance the infrared emissivity when their temperature is higher than the critical temperature and suppress the infrared emissivity when their temperature is below the critical temperature. The critical temperature depends on the phase-change temperature of VO_2, which can be adjusted by doping other elements into pure VO_2 [43]. First, Ono et al. proposed a concept of self-adaptive radiative cooling based on the combination of VO_2-based multilayer cooler and the top spectrally selective filter [38]. After that, Kim [39], Zhang [40], Kort-Kamp [41], and Liu

*Corresponding author: Yi Zheng, Department of Mechanical and Industrial Engineering, Northeastern University, Boston, MA 02115, USA; and Department of Chemical Engineering, Northeastern University, Boston, MA 02115, USA, E-mail: y.zheng@northeastern.edu.
https://orcid.org/0000-0003-4963-9684
Yang Liu, Department of Mechanical and Industrial Engineering, Northeastern University, Boston, MA 02115, USA

Open Access. © 2024 the author(s), published by De Gruyter. This work is licensed under the Creative Commons Attribution 4.0 International License.

[42] have successively proposed similar switchable radiative cooling systems based on the VO_2 photonic structures, all of which achieve radiative cooling at high ambient temperatures and keep their temperature around the ambient temperature at low temperatures. In addition, other types of switching radiative cooling systems also rely on mechanical switches [44]–[48], elastomeric modulators [49], [50], and temperature-sensitive material switches [51]–[53]. In fact, radiative cooling technology can only theoretically control the temperature of the cooling materials and cannot directly affect the indoor temperature due to a range of influencing factors, including wall thermal transfer, indoor ventilation, indoor lighting, indoor air conditioning, etc. In addition, achieving precise control of a constant indoor temperature becomes more challenging when relying solely on radiative cooling technology. Despite its potential to reduce energy consumption of indoor temperature regulation, passive radiative cooling technology has not yet reached a point where it can fully replace active air conditioning. Therefore, it is crucial to investigate the auxiliary effects of passive radiative cooling when combined with active indoor air conditioner–based temperature regulation, especially in terms of energy saving.

In this paper, we propose a VO_2-based radiative cooling system with the automatic reverse switching function that works in conjunction with the heating and cooling modes of indoor air conditioning to maintain a constant indoor temperature. Compared to conventional VO_2-based switching cooling structures, the reverse VO_2-based thermal system reduces its infrared emissivity (0.20) when its temperature exceeds the set temperature and increases the infrared emissivity (0.80) when its temperature falls below the set temperature, which is more suitable for use in conjunction with machine-based indoor air conditioning. Our proposed VO_2-based radiative cooling system synchronizes its cooling modes with the heating and cooling cycles of the indoor air conditioning during the actual process of precise temperature control. Additionally, we quantify the energy-saving potential of VO_2-based radiative technology in the precise control of indoor temperature. As a result, this work demonstrates the combination of the passive VO_2-based radiative thermal technology and the active air conditioning technology can pave the way for applications of precise indoor temperature control with significant energy-saving advantages.

2 Theoretical model and methods

Here, we propose a temperature control system integrating both active indoor air conditioning and passive radiative cooling, as schematically depicted in Figure 1. The passive radiative cooling component consists of the nanoporous polyethylene (NPE) [54] working as the top solar filter and the bottom VO_2-based double-layer film radiator. The structural parameters (thickness $h_{NPE} = 12$ μm and pore size $R_{pore} = 400$ nm) and infrared and visible transmittances of NPE can be found in the literature [54]. The bottom radiator consists of a VO_2 thin film ($h_1 = 150$ nm) deposed on a silicon dioxide (SiO_2) substrate with a thickness of 500 μm, tightly attached to the wall. More significantly in this work, the VO_2-based radiative cooling component in the entire system serves as an auxiliary element for precise temperature

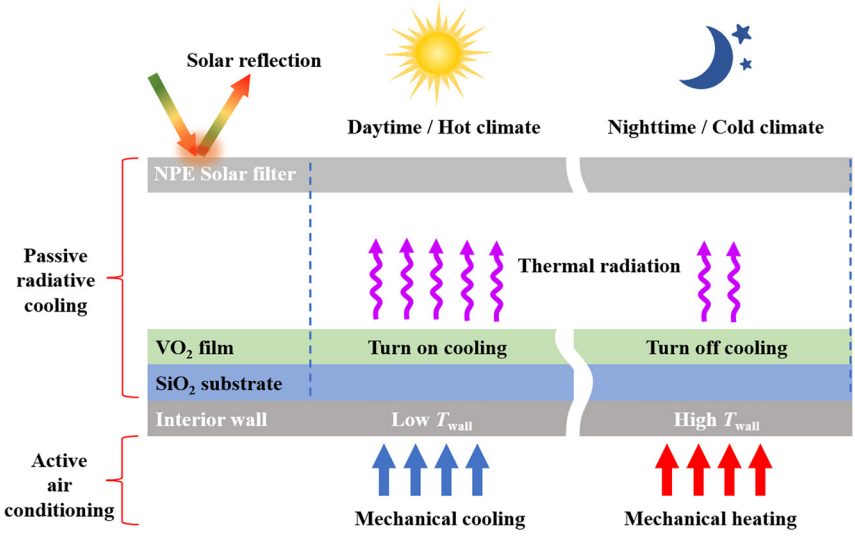


Figure 1: Design of the precise temperature control system that combines active indoor air conditioning and passive radiative cooling, where passive radiative cooling component consists of the top NPE and the bottom VO_2-based radiator.

control, aiming at reducing the energy consumption of air conditioning. The active indoor air conditioning component in Figure 1 adjusts its cooling and heating power according to the set of indoor temperature, playing a pivotal role in achieving precise temperature control.

Pure VO_2, a phase-change material, can achieve a reversible insulator-to-metal transition around 68 °C [55]. When the temperature of VO_2 is above the critical temperature T_c, VO_2 exhibits metallic behavior and changes to insulating state when its temperature falls below T_c. However, to broaden the application of VO_2's phase-change property, its T_c has been adjusted by doping other elements, such as molybdenum (Mo), tungsten (W), etc., into pure VO_2 to approach to the room temperature [43]. In this study, the permittivity of both metallic and insulating VO_2 during the wavelength range of 0.3 μm–15 μm is presented in Figure 2 [38]. Meanwhile, the phase-change process of VO_2 with temperature change is a gradual transition process in a narrow transition range $[T_c - \Delta T, T_c + \Delta T]$. To ensure precise temperature control in subsequent calculations, the dielectric function of VO_2 is defined as follows [39]:

$$\varepsilon_{\text{transition}} = \frac{\varepsilon_m + \varepsilon_i}{2} + \arctan\left(\frac{T - T_C}{\Delta T} \times 10\right) \times \left(\frac{\varepsilon_m - \varepsilon_i}{2 \arctan 10}\right), \tag{1}$$

where ε_m and ε_i are denoted as metallic and insulating permittivities, respectively. And the phase-change temperature of VO_2 is adjusted to $T_c = 20$ °C and $\Delta T = 0.1$ °C.

The thermal emissivity of the bottom VO_2-based radiative cooler in the spectral region ($\lambda \sim 0.3$–15 μm) is shown in Figure 3(a), where the red curve corresponds to the spectral emissivity of metallic-phase VO_2, and the blue line represents the spectral emissivity of the insulating-phase VO_2. It is clearly seen that, near the atmospheric transparent window

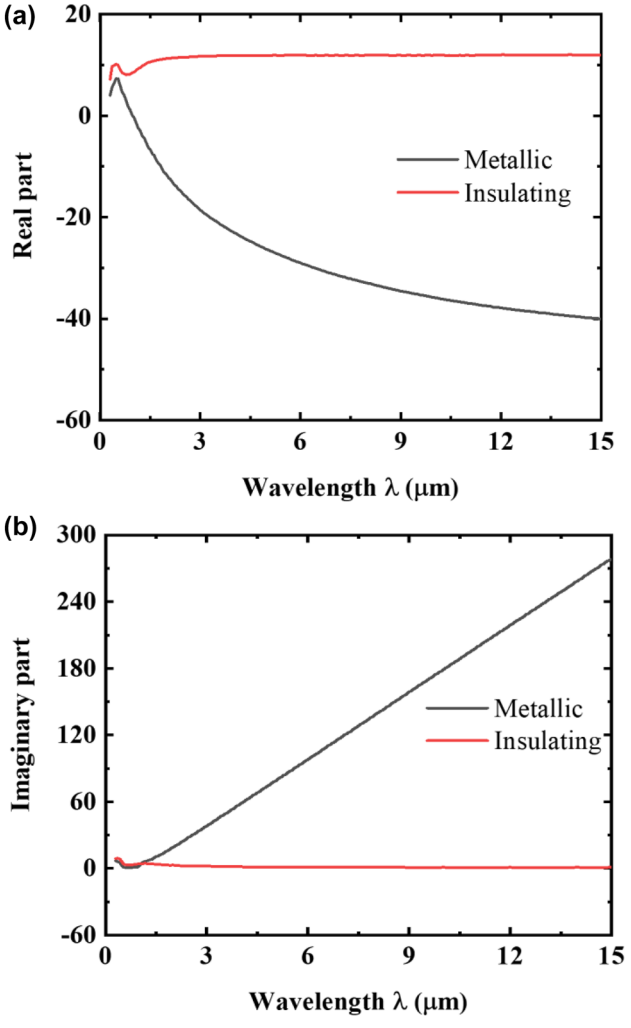


Figure 2: Optical properties of VO_2 at metallic and insulating states. (a) Real part and (b) imaginary part of VO_2 permittivity within the wavelength range (0.3–15 μm).

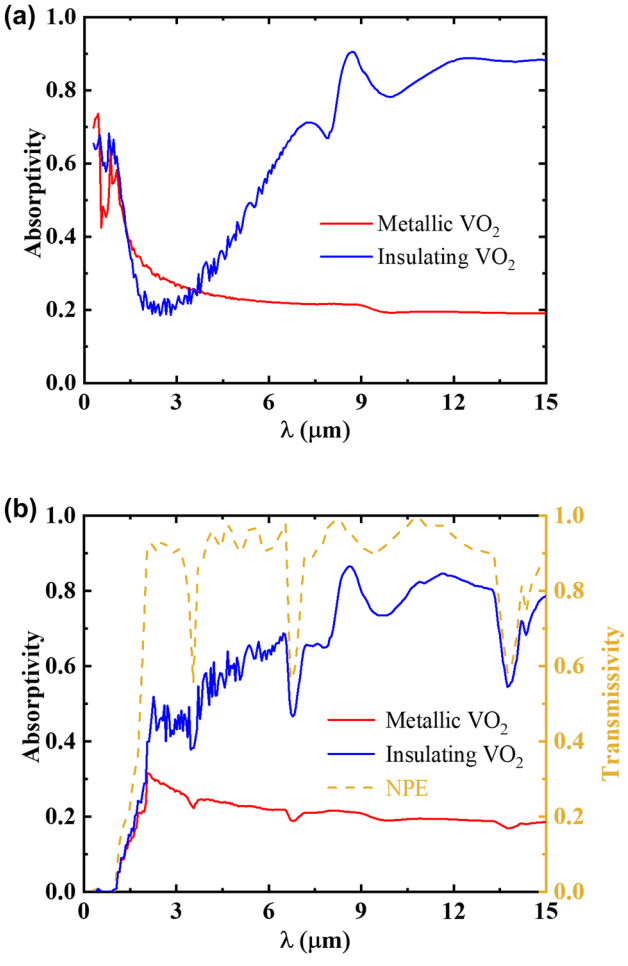


Figure 3: Emissivity of the VO_2-based radiative cooling system when VO_2 in metallic and insulating phases (a) without and (b) with the top NPE, respectively, as well as (b) spectral transmissivity of NPE.

($\lambda \sim 8$–13 μm), the spectral emissivity of VO_2-based radiative cooler at different states changes significantly. When the temperature of VO_2 is below T_c (insulating-state VO_2), the infrared emissivity of radiative cooler during the atmospheric window is 0.80. However, as the temperature of VO_2 rises above T_c (metallic-state VO_2), the infrared emissivity decreases substantially to 0.20. The increased temperature of VO_2-based radiative cooler can significantly suppress infrared emissivity, mainly due to the transition of VO_2 from insulator to metal around the critical temperature, as well as the associated infrared switching effect. Specifically, when the temperature of VO_2 is below T_c, the insulating-state VO_2 thin film exhibits high infrared transmittance. In this state, the emissivity of the VO_2-based radiative cooler is primarily determined by the broadband-emissive SiO_2 layer for radiative cooling. However, the VO_2-based radiative cooler demonstrates high solar absorptivity in both metallic and insulating states, mainly due to the intrinsic lossy characteristics of VO_2, which is not conducive to achieving significant switchable cooling regulation [38].

To eliminate this drawback, a layer of NPE with high solar reflectance and selective infrared transmission is placed atop the bottom VO_2 cooler with a certain distance, thereby blocking most solar irradiation from reaching the bottom structure while permitting the passage of most of the infrared radiation from the bottom cooler. Here, we employ incoherent calculations to determine the emissivity for the bottom cooler as follows [38], [56]:

$$\varepsilon(\lambda,\Omega) = (1-r_C)\left(t_N + t_N r_C r_N + t_N (r_C r_N)^2 + t_N (r_C r_N)^3 + \cdots\right) = t_N(1-r_C)/(1-r_C r_N) \quad (2)$$

where t_N and r_N are the transmissivity and reflectivity of NPE, respectively. And r_C is the reflectivity of the bottom VO_2-based radiative cooler [56]. After incorporating the top NPE, the emissivity of the composite VO_2-based cooling system within the same spectral region is depicted in Figure 3(b). Remarkably, the NPE effectively reduces solar absorption when VO_2 is in both metallic and insulating phases, while maintaining a significant difference in the infrared emissivity between the two phases of VO_2. This property contributes to create an ideal VO_2-based cooling system for its auxiliary functions in precise temperature control.

3 Results and discussion

When a radiative cooling system operates under a clear sky, the net cooling power Q_{net} is determined by solving the thermal balance equation, expressed as follows [6], [38], [57]:

$$Q_{net} = Q_{cooler}(T_{cooler}) - Q_{nr}(T_{amb}, T_{cooler}) - Q_{amb}(T_{amb}) - Q_{sun}(T_{cooler}) \quad (3)$$

where Q_{cooler} is the radiative power emitted from the radiative cooler, Q_{nr} is the nonradiative power, including the heat conduction and convection from the environment, and Q_{amb} and Q_{sun} represent the atmospheric radiation and sunlight absorbed by the cooler, respectively. Here, T_{amb} and T_{cooler} are the temperatures of ambient and radiative cooler, respectively. Q_{cooler}, Q_{nr}, Q_{amb}, and Q_{sun} can be described as below:

$$Q_{cooler}(T_{cooler}) = A\int_0^\infty \mathrm{d}\lambda I_{BB}(T_{cooler},\lambda)\varepsilon(\lambda,\theta,\phi,T_{cooler}) \quad (4)$$

$$Q_{nr}(T_{amb},T_{cooler}) = Ah_{nr}(T_{amb}-T_{cooler}) \quad (5)$$

$$Q_{amb}(T_{amb}) = A\int_0^\infty \mathrm{d}\lambda I_{BB}(T_{amb},\lambda)\varepsilon(\lambda,\theta,\phi,T_{cooler})\varepsilon(\lambda,\theta,\phi) \quad (6)$$

$$Q_{sun}(T_{cooler}) = A\int_0^\infty \mathrm{d}\lambda I_{AM1.5}(\lambda)\varepsilon(\lambda,\theta_{sun},T_{cooler}) \quad (7)$$

where A is the surface area of the radiative cooler, $I_{BB}(T_{cooler},\lambda) = 2hc^2\lambda^{-5}\exp(hc/\lambda k_B T - 1)^{-1}$ is the spectral blackbody radiance. In Eq. (7), $I_{AM1.5}(\lambda)$ represents the spectral irradiance intensity of solar irradiation at AM 1.5, and $\varepsilon_{atm}(\lambda,\theta) = 1 - t(\lambda)^{1/\cos\theta}$ is the atmospheric emissivity, in which $t(\lambda)$ stands for the atmospheric transmission coefficient in the zenith direction [6]. The nonradiative heat transfer coefficient is donated as h_{nr} (0–12 W/m^2/K), as seen in Eq. (5). Here, $h_{nr} = 8$ W/m^2/K is used throughout the calculations. A detailed explanation of the formula above can be referred to the literature [38], [58]. Finally, considering the heat transfer from indoor air conditioner to the radiative cooler, the time-dependent temperature of the radiative cooler can be obtained as follows:

$$C_{cooler}\frac{\mathrm{d}T}{\mathrm{d}t} = Q_{net}(T_{cooler},T_{amb}) + Q_{AC}. \quad (8)$$

where Q_{AC} represents the heat transfer from indoor air conditioner to the radiative cooler through heat conduction, and C_{cooler} is the heat capacitance of the radiative cooler.

Before coupling indoor air conditioning technology, we first analyze the dynamic cooling performance of the VO_2-based radiative cooling system by calculating its temperature under the typical 24-h outdoor weather condition with large temperature difference between day and night (July 20, 2018, in Stanford, California) [38]. Figure 4(a) displays the temperature variation of the VO_2-based radiative cooler

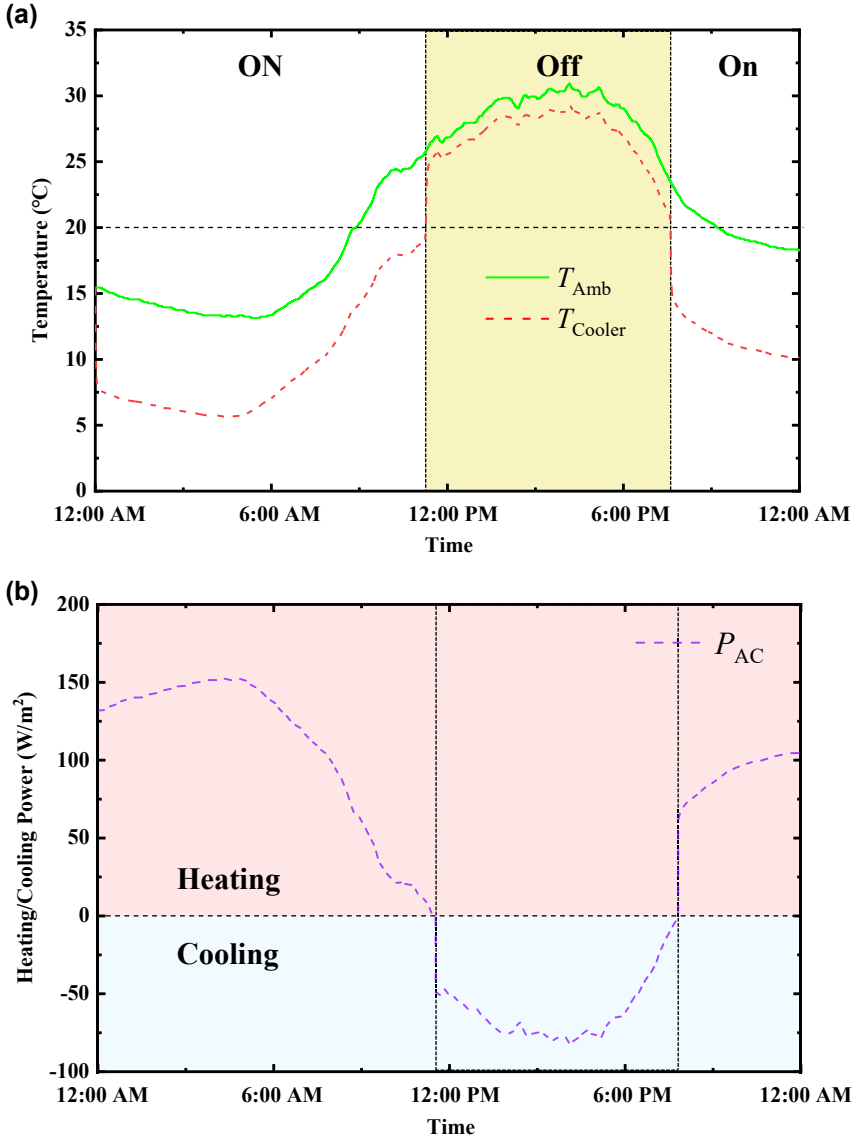


Figure 4: Thermal performance of the radiative cooling system and real-time heating and cooling power of the indoor air conditioner. (a) Temperature response of the VO_2-based radiative cooling system (red curve) over a 24-h cycle with varying ambient temperature (red curve). (b) Real-time heating and cooling power of the indoor air conditioner required to maintain the wall temperature at a constant 20 °C over the same 24-h period.

throughout a 24-h period without using air conditioning. Before 11:00 AM, the VO_2-based radiative cooler temperature is below the critical temperature 20 °C ($T < T_C$), the insulating-phase VO_2 enhances the infrared emissivity of VO_2-based radiative cooler, thereby turning on radiative cooling and creating a large temperature difference below the ambient temperature. Between 11:00 AM and 7:00 PM, when the temperature of the radiative cooler exceeds 20 °C ($T > T_C$), VO_2 turns to its metallic phase and then closes radiative cooling, which keeps its temperature near the variable ambient temperature. As a result, the single VO_2-based radiative cooler enhances radiative cooling under low ambient temperatures and suppresses cooling when the ambient temperature is high, thereby functioning as a reverse radiative "thermostat" [41]. This behavior can pose challenges in maintaining stable temperature control for objects. Without accounting for changes in the radiative characteristics of the outdoor VO_2-based radiative cooler caused by the heat transfer of the indoor air conditioner, Figure 4(b) illustrates the real-time heating and cooling power per area of the air conditioner required to maintain the wall temperature constant at 20 °C over the same 24-h period. Here, for

simplification in our calculations, we assume that the wall material is made of high thermal conductivity materials, with no heat loss, and the wall temperature equals the temperature of the VO_2-based radiative cooler. Figure 4(b) clearly shows that, when the wall temperature falls below the ambient temperature, the indoor air conditioner activates the heating mode, and when the wall temperature rises above the ambient temperature, the indoor air conditioner switches to cooling. After integrating over a 24-h period, the heating and cooling power per unit area of the wall to maintain a stable wall temperature at 20 °C, driven by the indoor air conditioner, amounts to 7,713,629 J/m^2.

In fact, different from the calculations mentioned above, in the precise control of wall temperature, the key factor affecting the spectral switching of the VO_2-based radiative cooler is the indoor air conditioner, rather than the ambient temperature. This is because the atmospheric radiation and the convective heat transfer from the ambient environment are far less significant than the direct cooling and heating provided by the indoor air conditioner. Under these conditions, indoor air conditioner directly affects the temperature of the VO_2-based radiative cooler through its heating and cooling actions, thereby regulating the infrared emissivity radiative cooler. As a result, both the indoor air conditioner and the outdoor VO_2-based radiative cooler operate in tandem to achieve temperature stabilization of the wall. As an example in this work, the focus is on precisely controlling the wall temperature around 20 °C. During the process of precise temperature control, the indoor air conditioner will first turn on the heating when the ambient temperature is below 20 °C, then raising the temperature of VO_2-based radiative cooler to around 20 °C. Conversely, the air conditioner turns on the cooling at high ambient temperatures, thereby reducing the temperature of the VO_2-based radiative cooler to around 20 °C. In order to play the role of a switchable VO_2-based radiative cooler in precise temperature control, two different heating and cooling cases for indoor air conditioning will be considered in the following calculations, as shown in Figure 5. Case 1 is that the air conditioner heats the temperature of the VO_2-based radiative cooler to 20.1 °C when the ambient temperature is below 20 °C and then cools it to 19.9 °C when the ambient temperature is above 20 °C. Case 2 is that the air conditioner heats the radiative cooler temperature to 19.9 °C and cools it to 20.1 °C under the same ambient temperature conditions, respectively. Based on the temperature distribution of VO_2-based radiative cooler assumed above, the real-time heating and cooling power of the air conditioner over the same 24-h period are calculated based on Eqs. (3)–(8), as seen in Figure 5. It is evident that, regardless of the heating

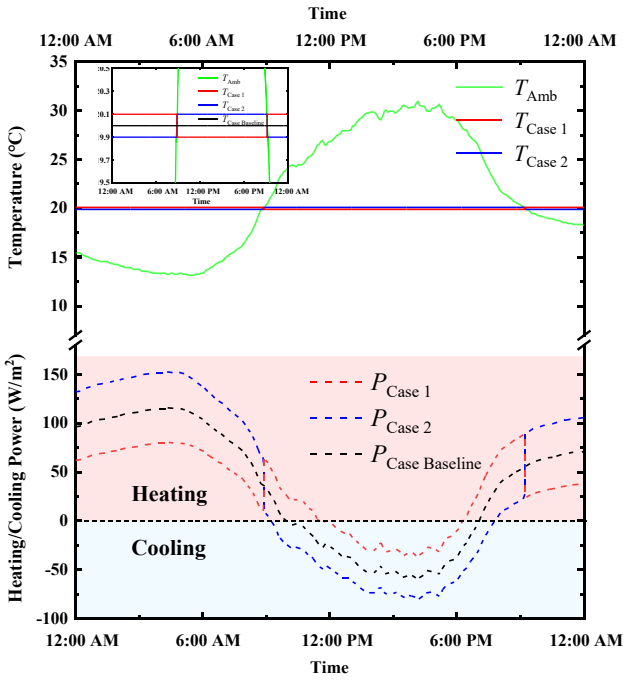


Figure 5: Wall temperature distributions in Case 1 and Case 2, as well as Case Baseline (without VO_2-based radiative cooling system), along with the corresponding real-time heating and cooling power of the indoor air conditioner to maintain the wall temperature around 20 °C over the same 24-h period.

or cooling stage for the indoor air conditioning, Case 2 consumes more energy than Case 1. In Case 1, the cooling operation of the VO_2-based radiative cooler is synchronized with the switching between heating and cooling modes of the air conditioner. When the air conditioner is in heating mode, the VO_2-based radiative cooler automatically turns off radiative cooling and then turns on radiative cooling when the air conditioner is in cooling mode. Conversely, in Case 2, the VO_2-based radiative cooler turns on radiative cooling when the air conditioner is in heating mode and turns off radiative cooling when the air conditioner is in cooling mode, thereby resulting in increased energy consumption by indoor air conditioners. Table 1 gives the detailed parameters of Case 1 and Case 2. Meanwhile, we also calculated the power consumption of the indoor air conditioner without any VO_2-based radiative cooling system for temperature regulation at 20 °C, referred to as Case Baseline, where the spectral emissivity of exterior wall is calculated by averaging the spectral emissivities of metallic VO_2 and insulating VO_2, as shown in Figure 1S. From Figure 5, under the condition of maintaining the wall temperature at 20 °C, the heating and cooling power consumed by indoor air conditioner within 24 h is 5,345,760 J/m^2 in Case Baseline

Table 1: Wall temperature distributions in Case 1 and Case 2 and the corresponding radiative cooling states of the reverse VO_2-based radiative cooler over the same 24-h period.

Case	T_{amb}	T_{cooler}	Air conditioner	Radiative cooling
Case 1	$T_{amb} < 20\,°C$	$T_{cooler} = 20.1\,°C$	Heating	Turn off
	$T_{amb} > 20\,°C$	$T_{cooler} = 19.9\,°C$	Cooling	Turn on
Case 2	$T_{amb} < 20\,°C$	$T_{cooler} = 19.9\,°C$	Heating	Turn on
	$T_{amb} > 20\,°C$	$T_{cooler} = 20.1\,°C$	Cooling	Turn off

and 7,335,583 J/m^2 in Case 2, which is nearly twice the value of Case 1, at approximately 3,782,783 J/m^2. Another outdoor weather condition on October 3, 2023, in Boston, MA, was also taken into consideration, as shown in Figure 2S. Compared with Case Baseline without switchable radiative cooling, the reverse VO_2-based radiative cooling system in Case 1 can substantially reduce the energy consumption by nearly 30 % for heating and cooling of indoor air conditioning, as calculated by (5,345,760−3,782,783)/5,345,760 = 30 %. In addition, comparing Case 1 and Case 2, the combination of passive switchable radiative cooling with active indoor air conditioning, coordinating their heating and cooling modes at the same frequency, results in significant energy savings during precise temperature control.

To further illustrate the energy-saving advantages of passive switchable radiative cooling technology during the precise temperature control dominated by indoor air conditioning, we compare the heating and cooling powers

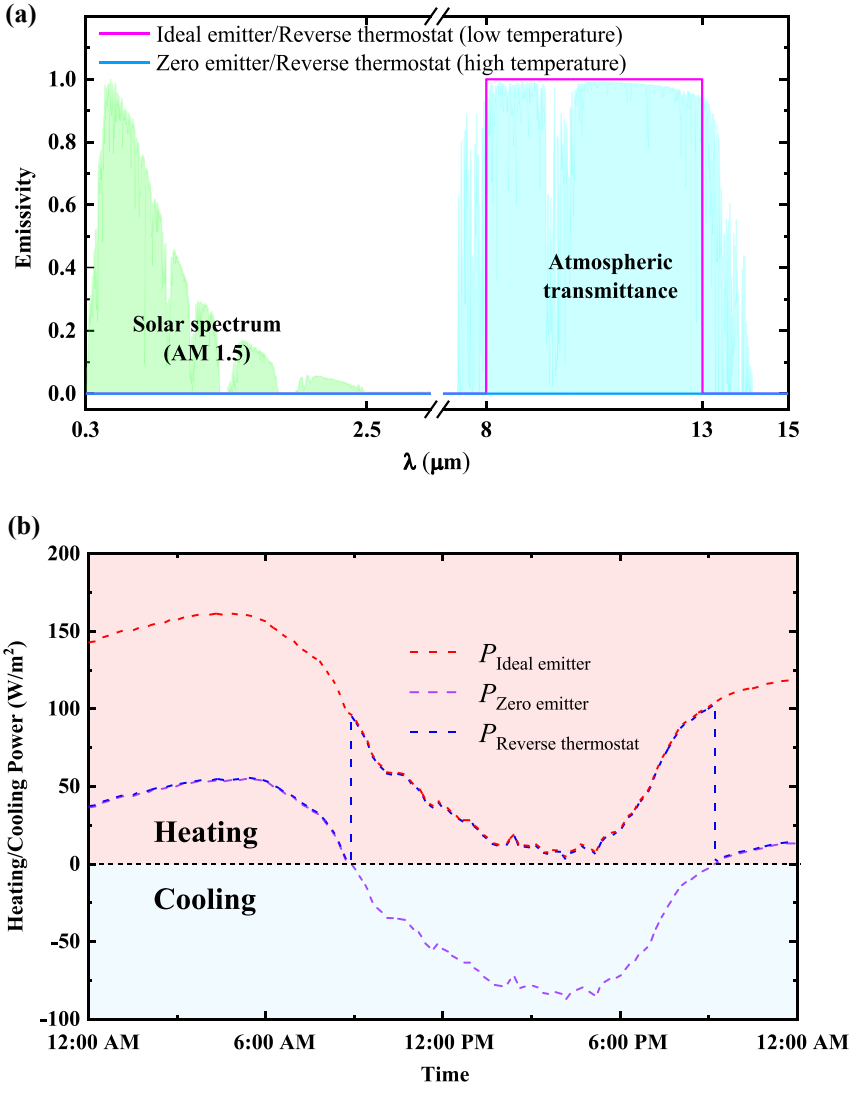


Figure 6: Comparison of three ideal radiators. (a) Emissivity comparison of the ideal emitter with one-value infrared emissivity, the zero emitter with zero-value infrared emissivity, and the ideal reverse thermostat with switchable one-zero-value infrared emissivity. (b) The corresponding real-time heating and cooling power required by the indoor air conditioner to maintain the wall temperature at 20 °C using these three radiators over the same 24-h period.

of the indoor air conditioner under three types of ideal radiators installed outside. Three ideal radiators include one-value infrared emissivity (ideal emitter), zero-value infrared emissivity (zero emitter), and switchable one-zero-value infrared emissivity (reverse thermostat). The spectral emissivity distributions for these radiators are shown in Figure 6(a). In this case, the ideal reverse thermostat exhibits an infrared thermal emissivity of 0 within the atmospheric transparent window (8–13 μm) at high temperature, while having an emissivity of 1 at low temperature. Similarly, the real-time heating and cooling powers of the air conditioner, maintaining the wall temperature around 20 °C, over the same 24-h period are calculated based on these three ideal radiators, as seen in Figures 6(b) and 3S. The heating and cooling powers used by the indoor air conditioner within 24 h are as follows: 7,705,658 J/m^2 (ideal emitter), 3,863,389 J/m^2 (zero emitter), and 3,300,983 J/m^2 (reverse thermostat), respectively. While the ideal emitter can maximize the radiative cooling power at higher ambient temperatures and the zero emitter can minimize the radiative cooling power at lower ambient temperatures, the energy expended by the air conditioning system with the ideal reverse thermostat remains the lowest among the daily accumulated energy consumption. This is due to the reverse thermostat synchronizes its cooling modes with the heating and cooling cycles of the indoor air conditioning, leading to minimal energy consumption by the indoor air conditioning system. Therefore, the above comparison further demonstrates that reverse radiative cooling system can effectively assist indoor air conditioners in reducing energy consumption during precise temperature control.

4 Conclusions

In conclusion, we propose and analyze a reverse-switching VO_2-based radiative cooling system, assisting indoor air conditioning to achieve precise indoor temperature control. Different from previous VO_2-based radiative cooling systems, our proposed VO_2-based radiative cooler automatically turns on radiative cooling at low ambient temperatures and turns off radiative cooling at high ambient temperatures. Rather than independently adjusting its infrared emissivity to stabilize indoor temperatures, the passive VO_2-based radiative cooling system synchronizes its cooling modes with the heating and cooling cycles of the indoor air conditioning during the real-life process of precise temperature control. The calculation results demonstrate that compared with the baseline system without switchable radiative cooling, the reverse VO_2-based radiative cooling system can substantially reduce the energy consumption by nearly 30 % for heating and cooling of indoor air conditioning while maintaining a constant indoor temperature, outperforming even the ideal radiative cooler. The precise temperature control is vital for achieving specific outcomes, maintaining product quality, ensuring equipment safety, and enhancing the human comfort. Therefore, this work will provide a potential application approach for radiative cooling technology and advance its intelligent thermal regulation alongside traditional air conditioning technology.

Research funding: This project was supported by the National Science Foundation through grant number CBET-1941743 and PHY-1748958.

Author contributions: YL initiated the project, developed the theory, conceived the approach, and performed simulations. YL and YZ supervised the project and wrote the manuscript. All authors analyzed the data and discussed the manuscript.

Conflict of interest: Authors state no conflicts of interest.

Data availability: The data that support the findings of this study are available from the corresponding author upon reasonable request.

References

[1] E. De Cian and I. Sue Wing, "Global energy consumption in a warming climate," *Environ. Resour. Econ.*, vol. 72, pp. 365—410, 2019.

[2] Y. Peng, *et al*., "Coloured low-emissivity films for building envelopes for year-round energy savings," *Nat. Sustain.*, vol. 5, no. 4, pp. 339—347, 2022.

[3] T. Li, *et al*., "A radiative cooling structural material," *Science*, vol. 364, no. 6442, pp. 760—763, 2019.

[4] S. S. Murshed and C. N. De Castro, "A critical review of traditional and emerging techniques and fluids for electronics cooling," *Renewable Sustainable Energy Rev.*, vol. 78, pp. 821—833, 2017.

[5] A. P. Raman, M. A. Anoma, L. Zhu, E. Rephaeli, and S. Fan, "Passive radiative cooling below ambient air temperature under direct sunlight," *Nature*, vol. 515, no. 7528, pp. 540—544, 2014.

[6] S. Fan and W. Li, "Photonics and thermodynamics concepts in radiative cooling," *Nat. Photonics*, vol. 16, no. 3, pp. 182—190, 2022.

[7] X. Yin, R. Yang, G. Tan, and S. Fan, "Terrestrial radiative cooling: using the cold universe as a renewable and sustainable energy source," *Science*, vol. 370, no. 6518, pp. 786—791, 2020.

[8] D. Zhao, *et al*., "Radiative sky cooling: fundamental principles, materials, and applications," *Appl. Phys. Rev.*, vol. 6, no. 2, p. 021306, 2019.

[9] Y. Zhai, *et al*., "Scalable-manufactured randomized glass-polymer hybrid metamaterial for daytime radiative cooling," *Science*, vol. 355, no. 6329, pp. 1062—1066, 2017.

[10] B. Zhao, M. Hu, X. Ao, N. Chen, and G. Pei, "Radiative cooling: a review of fundamentals, materials, applications, and prospects," *Appl. Energy*, vol. 236, pp. 489—513, 2019.

[11] X. Yu, J. Chan, and C. Chen, "Review of radiative cooling materials: performance evaluation and design approaches," *Nano Energy*, vol. 88, p. 106259, 2021.

[12] Y. Tian, *et al*., "Subambient daytime cooling enabled by hierarchically architected all-inorganic metapaper with enhanced thermal dissipation," *Nano Energy*, vol. 96, p. 107085, 2022.
[13] Z. Li, Q. Chen, Y. Song, B. Zhu, and J. Zhu, "Fundamentals, materials, and applications for daytime radiative cooling," *Adv. Mater. Technol.*, vol. 5, no. 5, p. 1901007, 2020.
[14] Q. Zhang, *et al*., "Recent progress in daytime radiative cooling: advanced material designs and applications," *Small Methods*, vol. 6, no. 4, p. 2101379, 2022.
[15] X. Wu, *et al*., "An all-weather radiative human body cooling textile," *Nat. Sustain.*, vol. 6, pp. 1446—1454, 2023.
[16] J. Lee, *et al*., "Biomimetic reconstruction of butterfly wing scale nanostructures for radiative cooling and structural coloration," *Nanoscale Horiz.*, vol. 7, no. 9, pp. 1054—1064, 2022.
[17] J. Yang, X. Zhang, X. Zhang, L. Wang, W. Feng, and Q. Li, "Beyond the visible: bioinspired infrared adaptive materials," *Adv. Mater.*, vol. 33, no. 14, p. 2004754, 2021.
[18] S. Jeong, C. Y. Tso, Y. M. Wong, C. Y. Chao, and B. Huang, "Daytime passive radiative cooling by ultra emissive bio-inspired polymeric surface," *Sol. Energy Mater. Sol. Cells*, vol. 206, p. 110296, 2020.
[19] N. N. Shi, C.-C. Tsai, F. Camino, G. D. Bernard, N. Yu, and R. Wehner, "Keeping cool: enhanced optical reflection and radiative heat dissipation in Saharan silver ants," *Science*, vol. 349, no. 6245, pp. 298—301, 2015.
[20] P. Yao, *et al*., "Spider-silk-inspired nanocomposite polymers for durable daytime radiative cooling," *Adv. Mater.*, vol. 34, no. 51, p. 2208236, 2022.
[21] J.-l.Kou, Z. Jurado, Z. Chen, S. Fan, and A. J. Minnich, "Daytime radiative cooling using near-black infrared emitters," *ACS Photonics*, vol. 4, no. 3, pp. 626—630, 2017.
[22] L. Zhou, *et al*., "A polydimethylsiloxane-coated metal structure for all-day radiative cooling," *Nat. Sustain.*, vol. 2, no. 8, pp. 718—724, 2019.
[23] A. Harrison and M. Walton, "Radiative cooling of TiO_2 white paint," *Sol. Energy*, vol. 20, no. 2, pp. 185—188, 1978.
[24] X. Li, J. Peoples, P. Yao, and X. Ruan, "Ultrawhite $BaSO_4$ paints and films for remarkable daytime subambient radiative cooling," *ACS Appl. Mater. Interfaces*, vol. 13, no. 18, pp. 21733—21739, 2021.
[25] X. Li, J. Peoples, Z. Huang, Z. Zhao, J. Qiu, and X. Ruan, "Full daytime sub-ambient radiative cooling in commercial-like paints with high figure of merit," *Cell Rep. Phys. Sci.*, vol. 1, no. 10, p. 100221, 2020.
[26] Y. Tian, *et al*., "Superhydrophobic and recyclable cellulose-fiber-based composites for high-efficiency passive radiative cooling," *ACS Appl. Mater. Interfaces*, vol. 13, no. 19, pp. 22521—22530, 2021.
[27] X. Xue, *et al*., "Creating an eco-friendly building coating with smart subambient radiative cooling," *Adv. Mater.*, vol. 32, no. 42, p. 1906751, 2020.
[28] P. Li, *et al*., "Thermo-optically designed scalable photonic films with high thermal conductivity for subambient and above-ambient radiative cooling," *Adv. Funct. Mater.*, vol. 32, no. 5, p. 2109542, 2022.
[29] M. A. Kecebas, M. P. Menguc, A. Kosar, and K. Sendur, "Passive radiative cooling design with broadband optical thin-film filters," *J. Quant. Spectrosc. Radiat. Transfer*, vol. 198, pp. 179—186, 2017.
[30] A. R. Gentle and G. B. Smith, "A subambient open roof surface under the Mid-Summer sun," *Adv. Sci.*, vol. 2, no. 9, p. 1500119, 2015.
[31] S. So, *et al*., "Highly suppressed solar absorption in a daytime radiative cooler designed by genetic algorithm," *Nanophotonics*, vol. 11, no. 9, pp. 2107—2115, 2021.
[32] S. K. Chamoli, W. Li, C. Guo, and M. ElKabbash, "Angularly selective thermal emitters for deep subfreezing daytime radiative cooling," *Nanophotonics*, vol. 11, no. 16, pp. 3709—3717, 2022.
[33] L. Zhu, A. Raman, and S. Fan, "Color-preserving daytime radiative cooling," *Appl. Phys. Lett.*, vol. 103, no. 22, p. 223902, 2013.
[34] E. Rephaeli, A. Raman, and S. Fan, "Ultrabroadband photonic structures to achieve high-performance daytime radiative cooling," *Nano Lett.*, vol. 13, no. 4, pp. 1457—1461, 2013.
[35] M. M. Hossain, B. Jia, and M. Gu, "A metamaterial emitter for highly efficient radiative cooling," *Adv. Opt. Mater.*, vol. 3, no. 8, pp. 1047—1051, 2015.
[36] Y. Jiang, *et al*., "Micro-structured polyethylene film as an optically selective and self-cleaning layer for enhancing durability of radiative coolers," *Nanophotonics*, vol. 12, no. 12, pp. 2213—2220, 2023.
[37] K. Sun, *et al*., "VO_2 metasurface smart thermal emitter with high visual transparency for passive radiative cooling regulation in space and terrestrial applications," *Nanophotonics*, vol. 11, no. 17, pp. 4101—4114, 2022.
[38] M. Ono, K. Chen, W. Li, and S. Fan, "Self-adaptive radiative cooling based on phase change materials," *Opt. Express*, vol. 26, no. 18, pp. A777—A787, 2018.
[39] M. Kim, D. Lee, Y. Yang, and J. Rho, "Switchable diurnal radiative cooling by doped VO 2," *Opto-Electron. Adv.*, vol. 4, no. 5, p. 05200006, 2021.
[40] W.-W. Zhang, H. Qi, A.-T. Sun, Y.-T. Ren, and J.-W. Shi, "Periodic trapezoidal VO_2-Ge multilayer absorber for dynamic radiative cooling," *Opt. Express*, vol. 28, no. 14, pp. 20609—20623, 2020.
[41] W. J. Kort-Kamp, S. Kramadhati, A. K. Azad, M. T. Reiten, and D. A. Dalvit, "Passive radiative "thermostat" enabled by phase-change photonic nanostructures," *ACS Photonics*, vol. 5, no. 11, pp. 4554—4560, 2018.
[42] Y. Liu, Y. Tian, X. Liu, F. Chen, A. Caratenuto, and Y. Zheng, "Intelligent regulation of VO_2-PDMS-driven radiative cooling," *Appl. Phys. Lett.*, vol. 120, no. 17, p. 171704, 2022.
[43] M. K. Dietrich, F. Kuhl, A. Polity, and P. J. Klar, "Optimizing thermochromic VO2 by co-doping with W and Sr for smart window applications," *Appl. Phys. Lett.*, vol. 110, no. 14, p. 141907, 2017.
[44] W. Yang, *et al*., "Engineering structural janus MXene-nanofibrils aerogels for season-adaptive radiative thermal regulation," *Small*, vol. 19, no. 30, p. 2302509, 2023.
[45] Z. Xia, Z. Fang, Z. Zhang, K. Shi, and Z. Meng, "Easy way to achieve self-adaptive cooling of passive radiative materials," *ACS Appl. Mater. Interfaces*, vol. 12, no. 24, pp. 27241—27248, 2020.
[46] X. Li, *et al*., "Integration of daytime radiative cooling and solar heating for year-round energy saving in buildings," *Nat. Commun.*, vol. 11, no. 1, p. 6101, 2020.
[47] J.-H. Wang, *et al*., "A superhydrophobic dual-mode film for energy-free radiative cooling and solar heating," *ACS Omega*, vol. 7, no. 17, pp. 15247—15257, 2022.
[48] Q. Zhang, *et al*., "Temperature-dependent dual-mode thermal management device with net zero energy for year-round energy saving," *Nat. Commun.*, vol. 13, no. 1, p. 4874, 2022.

[49] H. Fang, *et al*., "A triple-mode midinfrared modulator for radiative heat management of objects with various emissivity," *Nano Lett.*, vol. 21, no. 9, pp. 4106—4114, 2021.
[50] Z. Li, Y. Zhai, Y. Wang, G. M. Wendland, X. Yin, and J. Xiao, "Harnessing surface wrinkling—cracking patterns for tunable optical transmittance," *Adv. Opt. Mater.*, vol. 5, no. 19, p. 1700425, 2017.
[51] W. Zha, *et al*., "Nonvolatile high-contrast whole long-wave infrared emissivity switching based on In_3SbTe_2," *ACS Photonics*, vol. 10, no. 7, pp. 2165—2172, 2022.
[52] A. Heßler, *et al*., "In_3SbTe_2 as a programmable nanophotonics material platform for the infrared," *Nat. Commun.*, vol. 12, no. 1, p. 924, 2021.
[53] S.-R. Wu, K.-L. Lai, and C.-M. Wang, "Passive temperature control based on a phase change metasurface," *Sci. Rep.*, vol. 8, no. 1, p. 7684, 2018.
[54] P.-C. Hsu, *et al*., "Radiative human body cooling by nanoporous polyethylene textile," *Science*, vol. 353, no. 6303, pp. 1019—1023, 2016.
[55] Y. Liu, *et al*., "Ultrahigh-rectification near-field radiative thermal diode using infrared-transparent film backsided phase-transition metasurface," *Appl. Phys. Lett.*, vol. 119, no. 12, p. 123101, 2021.
[56] M. Large, D. McKenzie, and M. Large, "Incoherent reflection processes: a discrete approach," *Opt. Commun.*, vol. 128, nos. 4—6, pp. 307—314, 1996.
[57] P. Yang, C. Chen, and Z. M. Zhang, "A dual-layer structure with record-high solar reflectance for daytime radiative cooling," *Sol. Energy*, vol. 169, pp. 316—324, 2018.
[58] Y. Tian, L. Qian, X. Liu, A. Ghanekar, G. Xiao, and Y. Zheng, "Highly effective photon-to-cooling thermal device," *Sci. Rep.*, vol. 9, no. 1, pp. 1—11, 2019.

Supplementary Material: This article contains supplementary material (https://doi.org/10.1515/nanoph-2023-0699).